Nanoscale

PAPER

View Article Online
View Journal | View Issue

Cite this: *Nanoscale*, 2023, **15**, 18457

Tracking cellular uptake, intracellular trafficking and fate of nanoclay particles in human bone marrow stromal cells†

Mohamed Mousa, Yang-Hee Kim, Nicholas D. Evans, Richard O. C. Oreffo and Jonathan I. Dawson*

Clay nanoparticles, in particular synthetic smectites, have generated interest in the field of tissue engineering and regenerative medicine due to their utility as cross-linkers for polymers in biomaterial design and as protein release modifiers for growth factor delivery. In addition, recent studies have suggested a direct influence on the osteogenic differentiation of responsive stem and progenitor cell populations. Relatively little is known however about the mechanisms underlying nanoclay bioactivity and in particular the cellular processes involved in nanoclay-stem cell interactions. In this study we employed confocal microscopy, inductively coupled plasma mass spectrometry and transmission electron microscopy to track the interactions between clay nanoparticles and human bone marrow stromal cells (hBMSCs). In particular we studied nanoparticle cellular uptake mechanisms and uptake kinetics, intracellular trafficking pathways and the fate of endocytosed nanoclay. We found that nanoclay particles present on the cell surface as μm-sized aggregates, enter hBMSCs through clathrin-mediated endocytosis, and their uptake kinetics follow a linear increase with time during the first week of nanoclay addition. The endocytosed particles were observed within the endosomal/lysosomal compartments and we found evidence for both intracellular degradation of nanoclay and exocytosis as well as an increase in autophagosomal activity. Inhibitor studies indicated that endocytosis was required for nanoclay upregulation of alkaline phosphatase activity but a similar dependency was not observed for autophagy. This study into the nature of nanoclay-stem cell interactions, in particular the intracellular processing of nanosilicate, may provide insights into the mechanisms underlying nanoclay bioactivity and inform the successful utilisation of clay nanoparticles in biomaterial design.

Received 26th May 2023,
Accepted 21st September 2023

DOI: 10.1039/d3nr02447d

rsc.li/nanoscale

1. Introduction

Clay nanoparticles, also sometimes referred to as 2D nanosilicates, such as the synthetic hectorite LAPONITE® (herein "nanoclay") have shown exciting potential for applications in the biomedical field including in drug delivery[1,2] and regenerative medicine.[3–5] From a regenerative medicine perspective nanoclays have been applied in the design of nanocomposites to enhance the mechanical and biological properties of polymeric biomaterials and have also been extensively studied for their affinity for proteins and their utility as growth-factor delivery systems. In addition to their utility in biomaterial design, we and others have also reported the ability of nanoclay particles to directly induce, in cultured human bone marrow stromal cells, markers associated with osteogenic differentiation such as enhanced alkaline phosphatase activity, calcified bone nodule formation and upregulated expression of bone-related genes and proteins.[6,7] However, the mechanism(s) underlying this osteogenic bioactivity remains unclear. An important consideration is how nanoclay particles interact with cells in culture. In particular, are clay nanoparticles internalized by cells? If so, how and to what extent? Where are they transported within the cell and with which intracellular organelles do they co-localize? How does their internalization affect cell function? What is their intracellular fate, for example, are they degraded, released in the cytoplasm or exocytosed? The answers to these questions will give insight into nanoclay bioactivity and inform the application of these materials in biomaterial design.[8]

Bone & Joint Research Group, Centre for Human Development, Stem Cells & Regeneration, Faculty of Medicine, University of Southampton, Southampton, SO16 6YD, UK. E-mail: jid@soton.ac.uk

† Electronic supplementary information (ESI) available. See DOI: https://doi.org/10.1039/d3nr02447d

When nanoparticles reach the cell membrane, they enter the cell through various possible endocytosis mechanisms including phagocytosis, clathrin-mediated endocytosis, Caveolae-mediated endocytosis, clathrin/caveolae-independent endocytosis, and micropinocytosis.[8,9] Following endocytosis nanoparticles are normally found in membrane-bound endosomal/lysosomal vesicles although bare/free nanoparticles in the cytoplasm or other cell organelles such as nucleus, mitochondria and endoplasmic reticulum are occasionally reported.[9,10] This normally leads to significant alteration of cell functions such as viability, proliferation and differentiation. For example, endocytosis of nanoparticles such as gold and silica increase osteoblast differentiation through induction/stimulation of autophagy and colocalization with autophagosomes.[11,12]

Since the ability of nanoparticles, in general, to alter cell function is often dependent on their cellular uptake[13–15] we focussed first on the question of whether nanoclay particles were internalized by human bone marrow stromal cells and, if so, how, to what extent and at what rate. Previous studies have provided evidence that nanoclay particles are readily internalised *in vitro via* clathrin-mediated endocytosis by different stem cell types[6,16–18] (*e.g.* human mesenchymal stem cells & human adipose-derived stem cells). In the present study we sought to clarify, using a combination of confocal microscopy and inductively coupled plasma mass spectrometry (ICP-MS), the rate and kinetics of nanoclay cellular uptake and in particular the *in vitro* biodistribution of nanoclay particles in terms of the amount of particles endocytosed, adhered to the cell membrane or remaining in the extracellular space which may provide clues for how clay nanoparticles exert effects on cell phenotype *in vitro*.[19] We also set out to track the intracellular trafficking/transport pathway and fate of endocytosed nanoclay particles using transmission electron microscopy coupled to energy dispersive X-ray (TEM-EDX) to find evidence for whether clay nanoparticles degrade within cells, and how nanoclay particles may colocalize and possibly interfere with cell organelle(s)/pathway(s) which may underlie previously reported osteogenic effects.[13] Elucidating the intracellular fate of endocytosed nanoclay particles may offer new insights into possible mechanisms for nanoclay bioactivity.

2. Results

2.1. Effect of nanoclay on cell viability

We first confirmed the biocompatibility of nanoclay particles towards hBMSCs using WST-1 assay combined with microscopy of cells exposed to nanoclay for 24 hours. We first started with investigating whether the presence of nanoclay particles interfere with the WST-1 absorbance readout at 450 nm by directly adding nanoclay particles to the recovered cell culture media supernatants and we observed no significant interference (Fig. S1†). After confirming that the presence of nanoclay did not interfere with the WST-1 assay readout, we observed that nanoclay particles exhibited no/negligible effects on the metabolic activity of hBMSCs up to a dose of 100 μg mL^{-1} at varying cell densities (Fig. 1A). F-actin staining (FITC-phalloidin) and phase contrast microscopy confirmed normal cell spreading and morphology in the presence of Rhodamine B-labelled nanoclay particles which appeared associated with the cells in monolayer cultures (Fig. 1B and C).

2.2. Nanoclay uptake kinetics and mechanism

In order to track the extent and kinetics of nanoclay particle cellular uptake, confocal laser scanning microscopy was applied to position rhodamine-labelled nanoclay particles in relation to a cell mask-stained cell membrane as per a previous study by Mihaila *et al.*[16] As shown in Fig. 2, nanoclay particles are readily internalized by hBMSCs and within 24 h post-clay addition, almost all cells were observed to be positively stained for nanoclay. Higher magnification images showed that nanoclay was present both within the cell and on the cell membrane as aggregates of various sizes as well as being present extracellularly.

To quantify the percentage of nanoclay particles in (internalised), on (attached to the cell membrane) and outside the cell (free in the cell culture medium) we employed ICP-MS to quantify the distribution of nanoclay in various fractions of the cell culture system based on elemental analysis of lithium – a structural cation in the nanoclay crystal with relatively low background levels. Extracellular nanoclay was classed as that present within the recovered cell culture media, membrane associated nanoclay was classed as the fraction recovered following subsequent DPBS washes and internalized nanoclay was classed as the fraction remaining within the cellular fraction following the previous wash step (Fig. 3A).

In agreement with the confocal microscopy data, nanoclay cellular uptake exhibited a time-dependent significant increase ($P < 0.001$). At day 1 clay-cell contact time, around 15 pg of nanoclay particles were internalized per cell. Levels of internalization reached ~30 pg per cell at day 3 and doubled to ~60 pg per cell at day 7 (Fig. 3B). Regarding particle distribution in the cell culture system, around 98–99.3% of the initially applied clay particles remained within the cell culture media (not directly interacting with cells), while the conc. of internalized clay particles did not exceed 1.5% (Fig. 3C). Around 0.5% of total nanoclay applied was found attached/adhered to cell membrane as measured on the PBS washes during ICP-MS sample preparation.

Nanoclay cellular uptake has previously been reported to be *via* clathrin-mediated endocytosis.[16,18] Consistent with this, a clathrin-mediated endocytosis inhibitor chlorpromazine hydrochloride CPZ was applied at a concentration optimized to preserve hBMSC viability (5 μg mL^{-1}) as shown in Fig. 4A. CPZ significantly inhibited cellular uptake of rhodamine labelled nanoclay when observed by confocal microscopy (Fig. 4B).

Following confirming the ability of CPZ to block nanoclay uptake by hBMSCs, we set out to explore whether nanoclay endocytosis plays a significant role in it's ability to upregulate alkaline phosphatase activity – a key early marker for osteogenesis which is known to be strongly upregulated by nanoclay

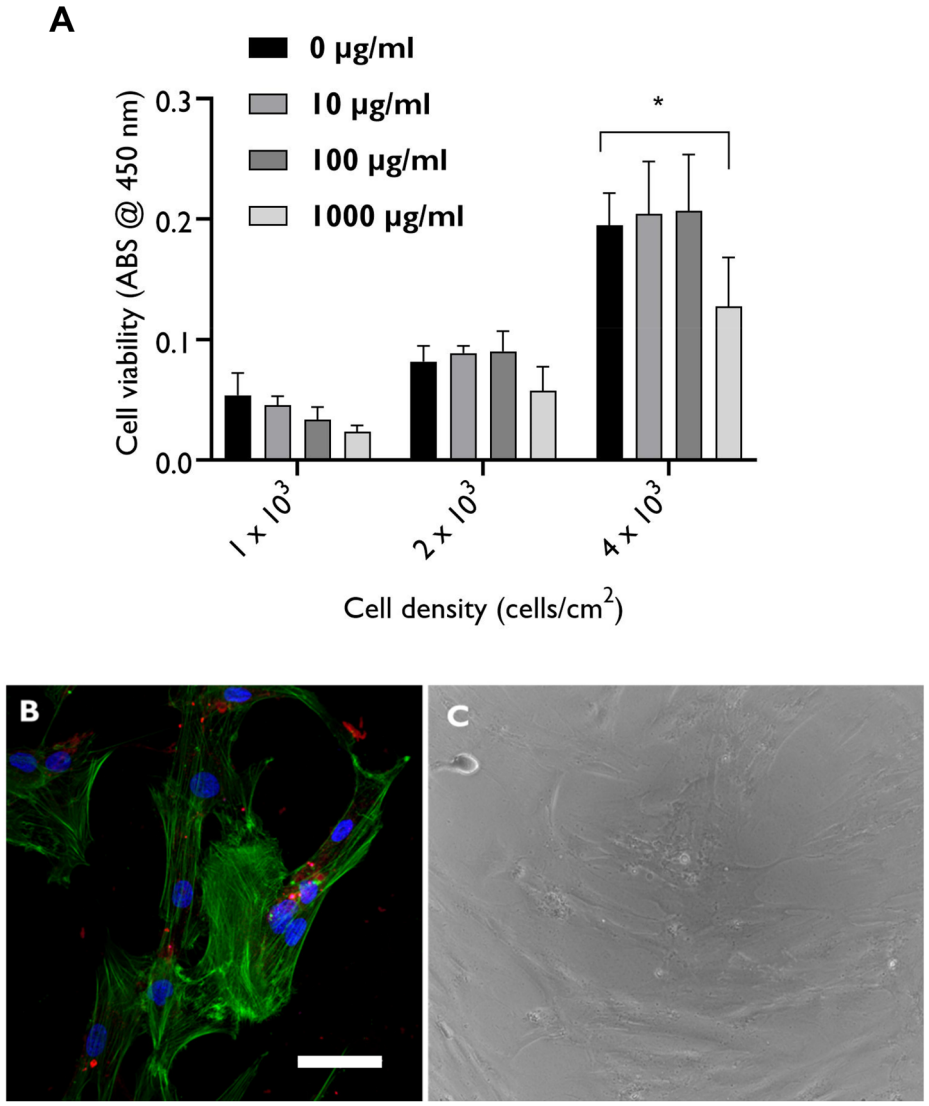

Fig. 1 Effect of nanoclay on hBMSCs viability and attachment. Nanoclay particles are cytocompatible up to a conc. of 100 µg ml^{-1} as shown by unaltered cell metabolic activity (A) and preserved cell attachment (B&C). Scale bar = 50 µm. Red (RB-labelled nanoclay particles); green (F-actin stained with FITC-phalloidin); blue (nucleus). Statistical analysis was performed using two-way ANOVA followed by Tukey's multiple comparisons test. Data represent mean ± SD, N = 3 experimental replicates. *$P < 0.05$.

addition.[20] Significantly, we found that inhibiting nanoclay endocytosis effectively attenuates the dose-dependent upregulation of alkaline phosphatase activity with nanoclay addition in both basal and osteogenic media. This provides an interesting indication that, despite the relatively low fraction taken up by cells, endocytosis is indeed necessary for the dose-dependent effects of nanoclay on osteogenic markers (Fig. 4C).

2.3. Tracking intracellular journey and fate of nanoclay

Given the importance of endocytosis for nanoclay upregulation of ALP activity, we undertook TEM analysis to study the interactions and fate of nanoclay within cells. Under TEM, nanoclay disks present as spindles of about 30 nm length due, presumably, to their low mass thickness contrast when viewed parallel to the planar surface. Recent work by Carrow *et al.* and Cross *et al.* reported disc shaped nanoclay particles with an average particle size of 50 nm as shown by TEM and zeta potential of −25 mV in biological media.[18,21] Particles were observed distributed both extracellularly and intracellularly in the form of clusters/aggregates of around 0.2–2 µm diameter (Fig. 5). Visual identification of nanoclay was also confirmed by EDX analysis which detected silicon and magnesium peaks in the clay-treated groups but not in the clay-free control. In agreement with the confocal microscopy and ICPMS data, the internalized clay aggregates increased in size and number between day 3 to day 7 and were found distributed throughout the cytoplasm from the perinuclear region to near the plasma membrane. No nanoclay particles were detected inside the nucleus.

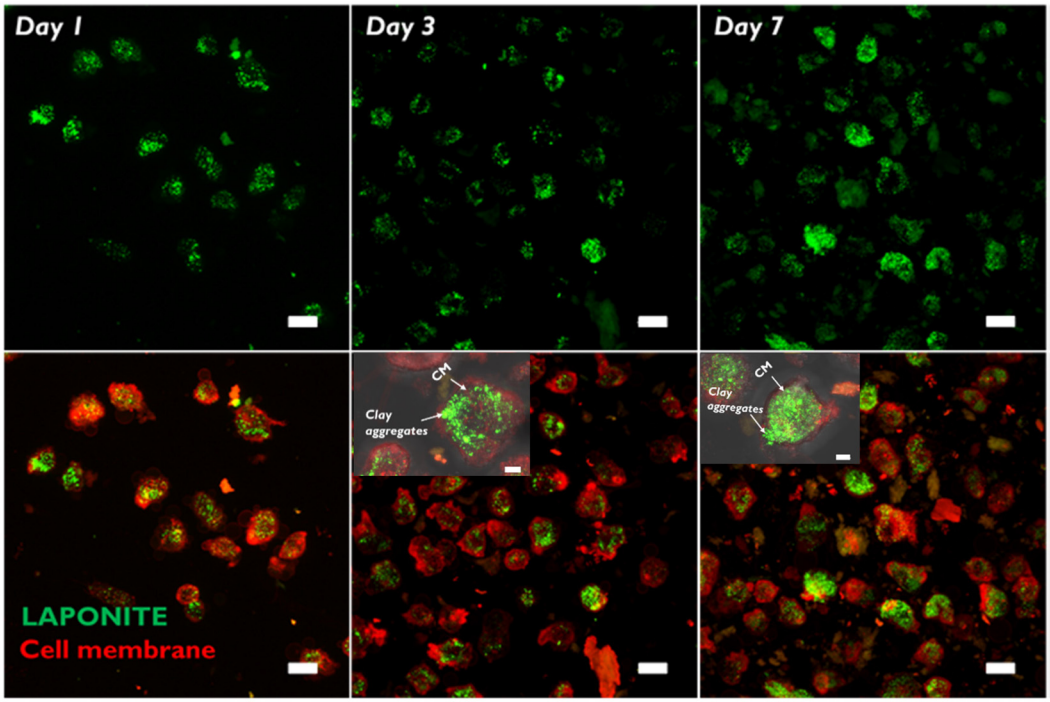

Fig. 2 Tracking cellular uptake of nanoclay particles by confocal microscopy. nanoclay exhibit strong affinity for internalization by hBMSCs in a time-dependent manner. Scale bar = 20 μm. Arrows in magnification confocal imaging demonstrate interaction of nanoclay with hBMSCs as perinuclear aggregates of various sizes distributed across the cell. Green (RB-labelled nanoclay particles); red (cell mask-stained plasma membrane). Scale bar = 5 μm.

Endocytosis of nanoclay could be observed by the formation of cellular protrusions engulfing clay aggregates proximal to the plasma cell membrane (Fig. 6). Nanoclay particles at this stage are around 30–50 nm in size. Within the cell, nanoclay particles could be observed within numerous membrane-bound endosomal compartments of early maturation stage[22] and in these compartments particles typically displayed a similar particle size and morphology to nanoclay particles observed outside the cell. Nanoclay particulates and corresponding Si and Mg EDX peaks were also observed within relatively electron-dense lysosomal bodies containing intraluminal vesicles. In lysosome compartments, particularly those intensely stained for osmium which is indicative of a mature lysosome, it is notable that the number of intact nanoclay particles significantly decreased. This is reflected in an overall decrease in particles size (<10 nm) and also, interestingly, an increase in the EDX peak ratio of Si to Mg compared to extracellular and endosomal clay. This is evidence of intracellular degradation of nanoclay particles in lysosomes corresponding with endo-/lysosomal maturation.

Finally, it was also possible to observe secretory lysosomal vesicles containing nanoclay, again confirmed by EDX analysis, apparently fusing with the plasma membrane. This suggests that, in addition to lysosomal degradation, exocytosis of vesicles containing nanoclay particles may also be a feature of the cellular response to internalized clay (Fig. 7).

2.4. Cell response to nanoclay internalisation

A prominent feature of nanoclay treated cells was the presence of double membrane-bound vesicles which were not observed in the control. A double membrane is a defining feature of autophagosomes and autolysosomes. The majority of such autophagosomes contained lamellar/residual bodies and fused with clay-lysosomes for autolysosome formation potentially for clay and organelle degradation (Fig. 8A). In agreement with TEM data, western blot analysis confirmed a stimulatory effect of nanoclay on hBMSCs autophagy as shown by nanoclay-enhanced expression of autophagy proteins: microtubule-associated protein light chain 3 (LC3) and p62 (Fig. 8B).

Finally, we sought to investigate whether the observed effect of nanoclay on ALP activity was dependent on autophagy activation. To test this link we applied a well-established autophagy inhibitor 3-methyladenine 3-MA that inhibits the formation of autophagosomes by inhibiting the class III phosphatidyl inositol 3-kinase.[11] 3-MA was successful in attenuating the nanoclay associated upregulation of autophagy markers LC3 and P62. We next tested the effect of 3-MA (0.5 mM) on nanoclay induced upregulation of alkaline phosphatase activity. Notably, despite the ability to inhibit autophagy, co-addition of the inhibitor with nanoclay failed to significantly attenuate the nanoclay-induced upre-

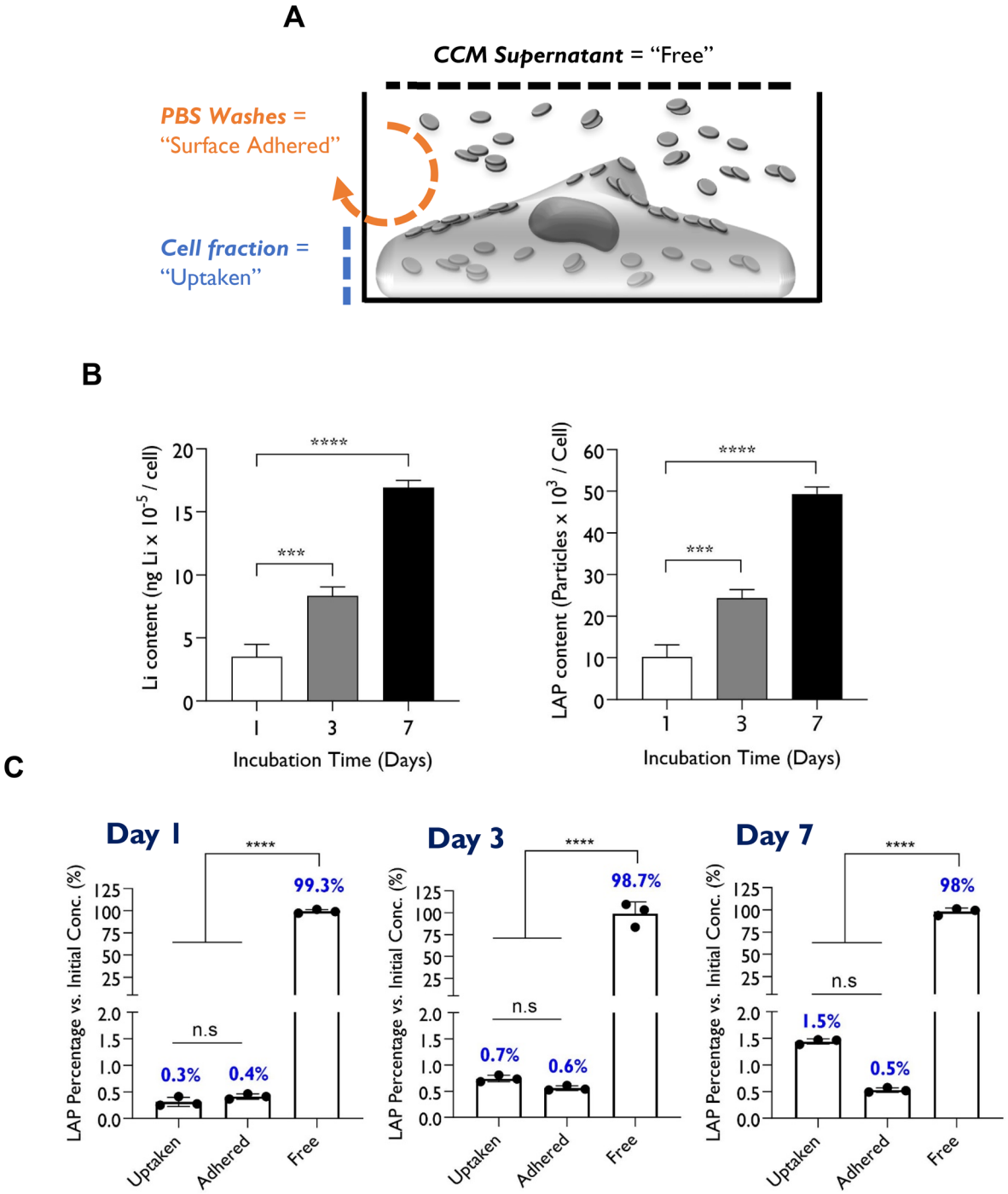

Fig. 3 Cellular uptake kinetics and distribution of nanoclay (LAP) across the cell culture system. (A) Schematic representation demonstrating the approach adopted for quantifying nanoclay particles *in vitro*; in, on and outside the cell. (B) The profile of nanoclay particles taken up by cells increases in a time-dependent manner from 15 pg LAP per cell at day 1 to 60 pg LAP per cell at day 7. (C) The vast majority of the nanoclay particles applied to cells remained in the extracellular space (98–99%) and only below 1.5% were internalized by cells. Statistical analysis was performed using one-way ANOVA followed by Tukey's multiple comparisons test. Data represent mean ± SD, $N = 3$. ***$P < 0.001$; ****$P < 0.0001$; n.s = non-significant.

gulation of ALP activity. This suggests against a direct association between these two responses to nanoclay addition under the conditions tested in this study (Fig. 8B and C).

3. Discussion and analysis

In this study the interactions between nanoclay particles and hBMSCs were tracked in terms of nanoclay uptake kine-

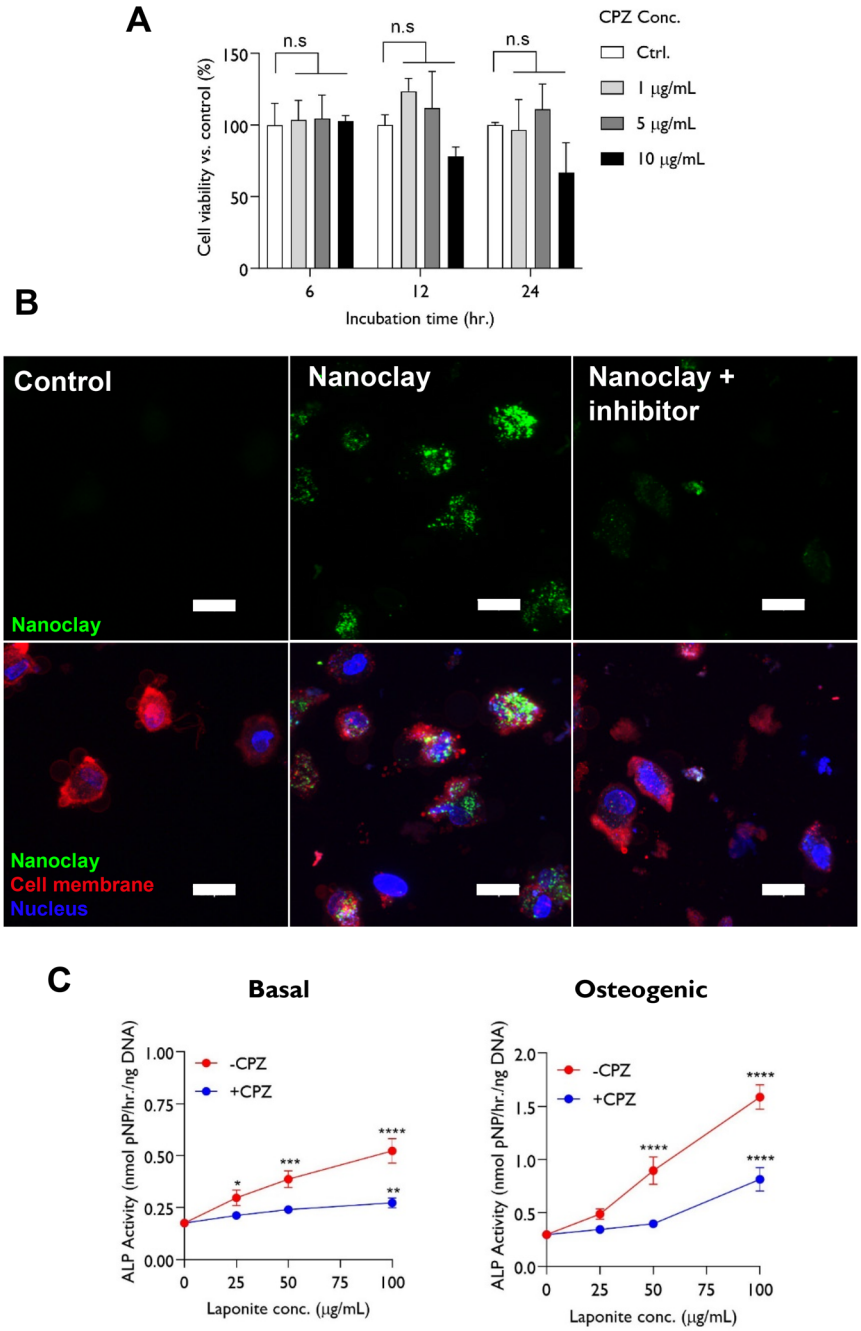

Fig. 4 Effect of endocytosis inhibitor chlorpromazine hydrochloride on nanoclay cellular uptake and ALP activity of hBMSCs. (A) CPZ was cytocompatible up to a dose of 5 μg mL^{-1} which was selected for assessing mechanism of nanoclay uptake. (B) CPZ significantly reduced nanoclay uptake by hBMSCs indicative of clathrin mediated endocytosis. Cells were incubated with RBITC-labelled nanoclay dispersions in presence or absence of 5 μg mL^{-1} CPZ for 24 h and particle internalization was visualized by confocal microscopy through *z*-stacking of detached cell suspension. Scale bar = 20 μm. (C) Blocking nanoclay endocytosis resulted in significant attenuation of nanoclay-induction of ALP activity at day 3 across the nanoclay dose range tested, implying that nanoclay endocytosis is crucial for its osteogenic character reflected in ALP activity. Statistical analysis was performed using two-way ANOVA followed by Tukey's multiple comparisons test. Data represent mean ± SD, $N = 3$. *$P < 0.05$; ****$P < 0.0001$; n.s = non-significant.

tics and mechanism, *in vitro* distribution, intracellular trafficking and fate and nanoclay influence on cell autophagy as well as effect of autophagy inhibition on nanoclay bioactivity. Nanoclay was readily internalized by hBMSCs *via* clathrin mediated endocytosis with kinetics following a linear increase with incubation time, but did not reach saturation level even after 7 days of nanoclay exposure. Notably, inhibition of endocytosis was sufficient to suppress

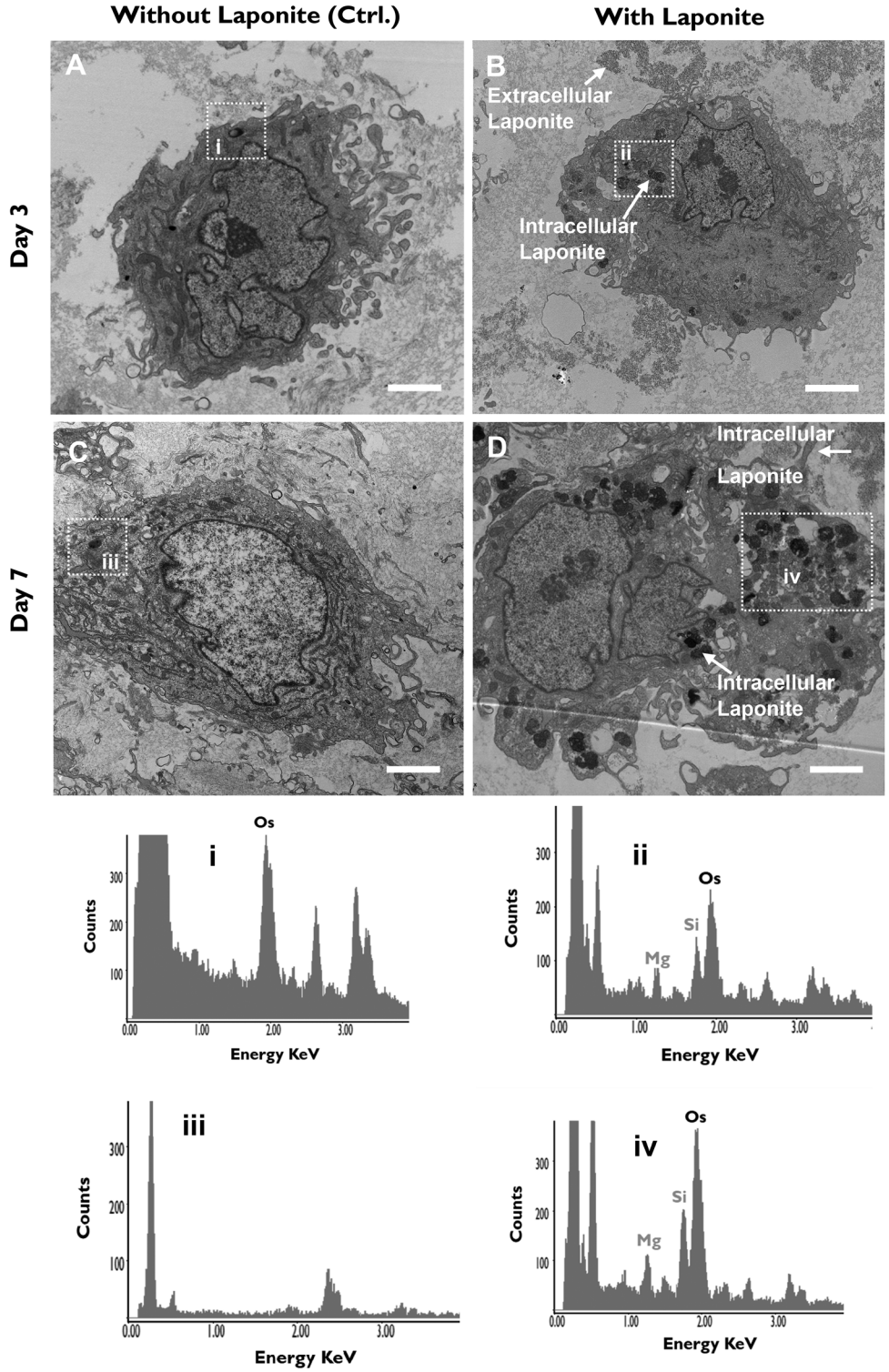

Fig. 5 Cellular uptake kinetics and extracellular *vs.* intracellular distribution of nanoclay. Cells were cultured, alongside controls (A & C) with 100 μg mL^{-1} nanoclay dispersion (B & D) for 3 (A & B) and 7 (C & D) days. nanoclay particles were found both extra- and intracellularly in the form of aggregates/clusters which increased in number with incubation time. Intracellular nanoclay aggregates distributed throughout the cytoplasm. EDX analysis of areas i and iii confirm absence of nanoclay in nanoclay-free cells while areas ii and iv confirm presence of nanoclay in cell lysosomes in days 3 and 7 post-nanoclay addition, respectively. Images were taken at low magnifications of 6000×, using FEI Tecnai T12 Transmission Electron Microscope at 80 kV voltage. Scale bar = 2 μM. Boxes represent nanoclay-free (i & iii) *vs.* nanoclay-containing (ii & iv) lysosomes.

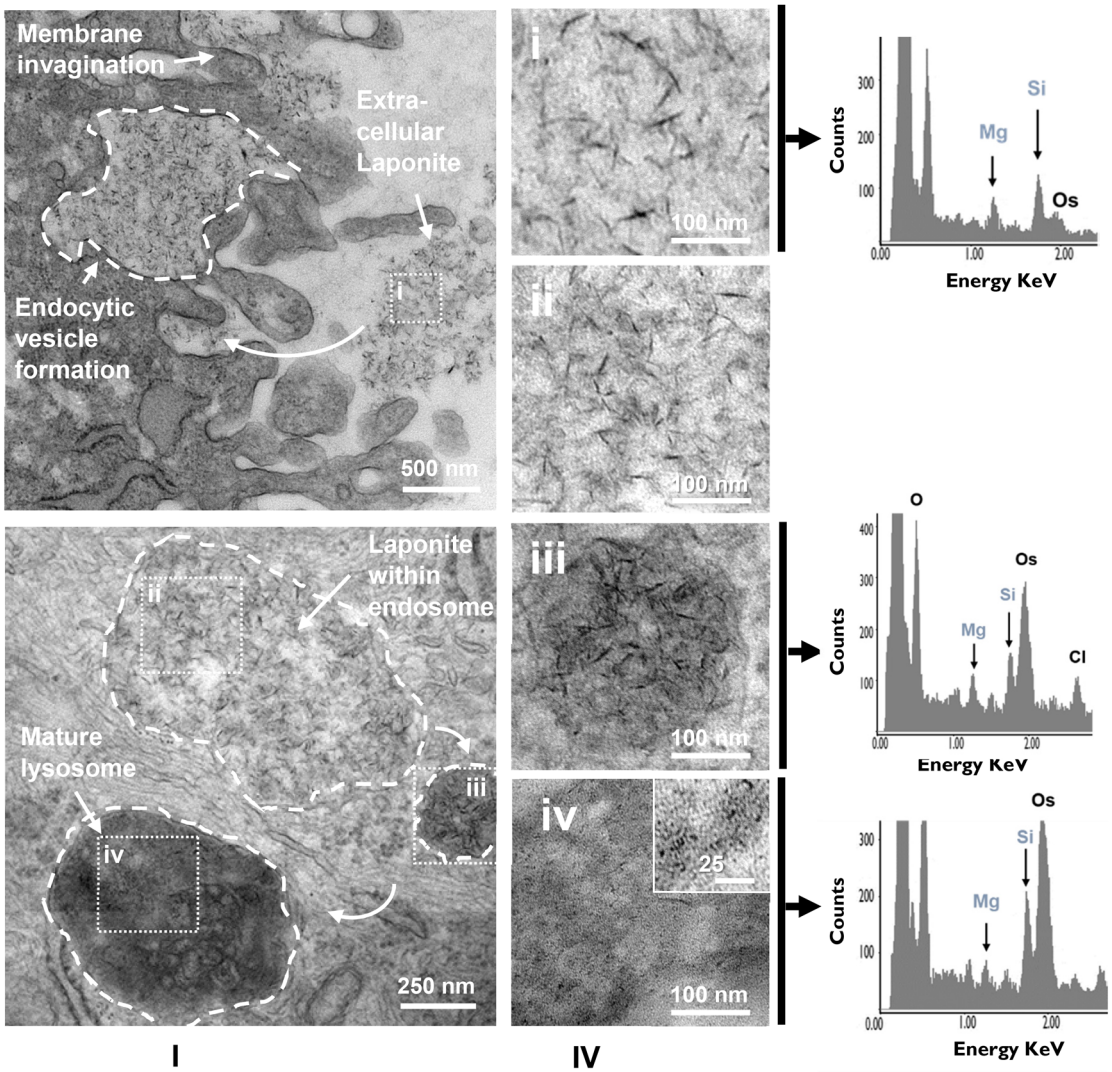

I

Element	Weight %	Atomic %
SiK	0.8	0.4
MgK	0.4	0.2
Si/Mg	2	2

IV

Element	Weight %	Atomic %
SiK	1.5	0.8
MgK	0.4	0.3
Si/Mg	3.8	2.7

Fig. 6 Intracellular fate of endocytosed nanoclay particles. nanoclay particles are endocytosed for subsequent entrapment within endosomal/lysosomal compartments and eventual degradation reflected in decrease in particle size and increase in Si/Mg ratio. Cells were treated with 100 μg mL^{-1} nanoclay dispersion for 7 days. Images were taken using FEI Tecnai T12 Transmission Electron Microscope at 80 kV voltage. L = lysosome; PM = plasma membrane. i refers to extracellular (intact) nanoclay particles (~30–50 nm), ii represent nanoclay particles in endosomes, iii shows nanoclay particles in lysosomes with higher degree of vesicle maturity and iv represents nanoclay particles undergoing degradation within lysosomal bodies reducing nanoclay particle size to <10 nm. EDX analysis of areas i and iv suggests nanoclay degradation as shown by increased Si/Mg peak ratios in response to nanoclay uptake and processing within lysosomal bodies.

the nanoclay induced upregulation of alkaline phosphatase activity – an early osteogenic marker.

Nanoclay particles were found both extracellularly, intracellularly as well adhered on plasma membrane as clusters/aggregates with the extracellular portion representing the vast majority of initially applied nanoclay particles. The formation of these nanoclay aggregates is attributed to the high ionic strength of cell culture media and the presence of serum proteins which induces an increase in edge-face interactions and the formation of nanoclay-protein complexes.[7,23,24] Nanoclay started its intracellular journey through interaction with plasma membrane as clusters which were subsequently endocytosed and entrapped within endosomal/lysosomal vesicles. These nanoclay/lysosomal compartments were distributed throughout the cytoplasm from the perinuclear to the peripheral regions and in some cases fused with the cell membrane. No nanoclay particles were observed free in the cytoplasm or in any other cell organelle such as nucleus, mito-

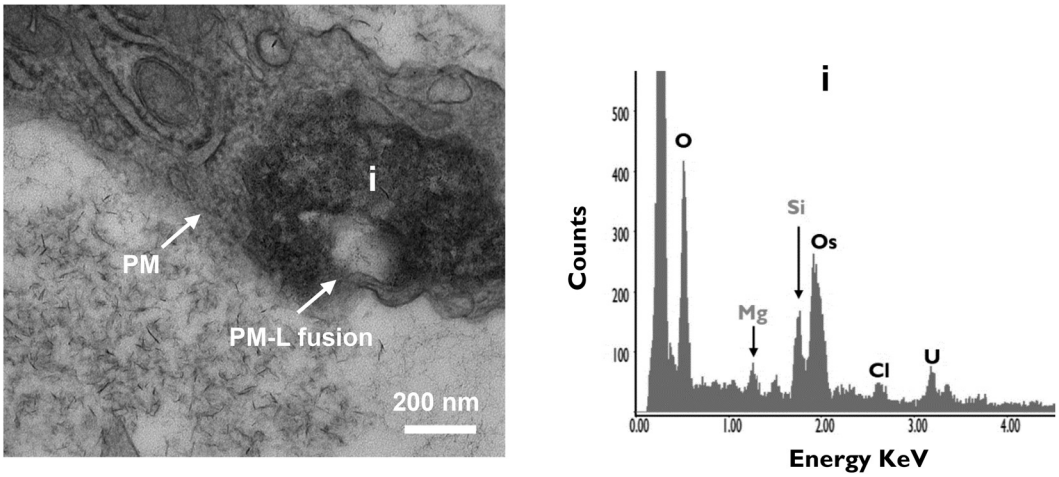

Fig. 7 Potential exocytosis of processed/degraded nanoclay particles. nanoclay-containing lysosomal bodies were found fused with plasma membrane indicating exocytosis of degraded nanoclay particles. Cells were treated with 100 μg mL^{-1} nanoclay dispersion for 7 days then fixed and imaged using FEI Tecnai T12 Transmission Electron Microscope at 80 kV voltage. Scale bar = 200 nm. EDX analysis confirm presence of nanoclay elemental peaks (Si & Mg) in selected area i. PM = plasma membrane; L = lysosome.

chondria, endoplasmic reticulum or Golgi apparatus. TEM-EDX analysis suggested intracellular dissolution and exocytosis of internalized nanoclay particles through endosomal-lysosomal maturation stages. On the other hand, the cell physiological behaviour was significantly affected by nanoclay endocytosis as evidenced by induced/enhanced autophagy.

When in contact with hBMSCs, nanoclay was readily internalized and appeared well distributed almost across the cytoplasmic region. Nanoclay endocytosis is expected given the physicochemical properties of nanoclay which give it a strong affinity for cellular uptake.[4] For example, the cationic edge charge of nanoclay ($Si–OH_2^+$) allows direct/electrostatic interaction with the anionic glycoproteins and phospholipids of the cell membrane and thus may also facilitate nanoclay cellular interaction and uptake.[15,16,25,26] Furthermore, studies of the effect of nanoparticle size on endocytosis have identified the optimal particle size for cellular endocytosis is in the order of 25–30 nm.[27] This corresponds exactly with the surface plane of nanoclay (25–30 nm sheets).[21,28] However it is notable that nanoclay particles present on the cell surface as micrometer sized aggregates rather than as individual platelets and so the specific relevance of the particle unit size for uptake efficiency in this case is not clear. The fact nanoclay interacts with the cell membrane as aggregates is itself likely to play a role in the process of internalisation. For example, several studies indicate that nanoparticle clusters may have a higher chance and rate of internalization than single/individual nanoparticles as for example the case of silica nanoparticles.[8,29,30] Jin *et al.* developed an interesting model which showed that nanoparticles diffuse to/on the cell membrane to form aggregates with a size sufficient to generate a driving force that can overcome the elastic energy and entropic barriers associated with endocytosis[31] – something that does not occur with single particles.[11]

Overall, these results agree with various recent studies which reported a strong affinity of nanoclay for interaction with various cell types including stem and cancer cell models. For example, nanoclay was readily internalized by human mesenchymal stem cells within 5 minutes[18] and enhanced the antitumor efficacy of DOX drug primarily due to the observed increase in cellular uptake of a nanoclay/DOX complex than that of free DOX.[32]

Next, we moved to track the kinetics of nanoclay cellular uptake which is scarcely explored in literature. It was observed that while the amount of internalized nanoclay particles increases linearly with time, it does not appear to reach saturation level even at day 7 of nanoclay addition. Interestingly these data contrast with flow cytometry analysis presented by Carrow *et al.* – the only study reporting nanoclay uptake kinetics which implied a more rapid association of nanoclay particles with cells reaching saturation at only 5 min post-nanoclay addition.[18] This might be attributed to various experimental factors such as the method of nanoclay-culture media preparation, cell type and seeding density.[8] Furthermore, such variation could be attributed to the technique used for quantifying number of endocytosed particles per cell. We relied on ICPMS for nanoparticle quantification while Carrow *et al.* used flow cytometry. While the first is a sensitive tool based on label-free elemental analysis, the second is limited by the background of particle aggregation and dye leaching.

Following endocytosis, nanoclay particles/aggregates were observed entrapped within membrane bound endosomal/lysosomal vesicles – a similar intracellular trafficking pathway observed for various nanoparticles including gold,[33,34] silica,[12] silver[35] and anionic nanoclays.[36] Some of these vesicles were found in close proximity in the juxtanuclear region with different levels of electron density suggesting late endosome-lysosome fusion.[37] We did not detect clay particles in the

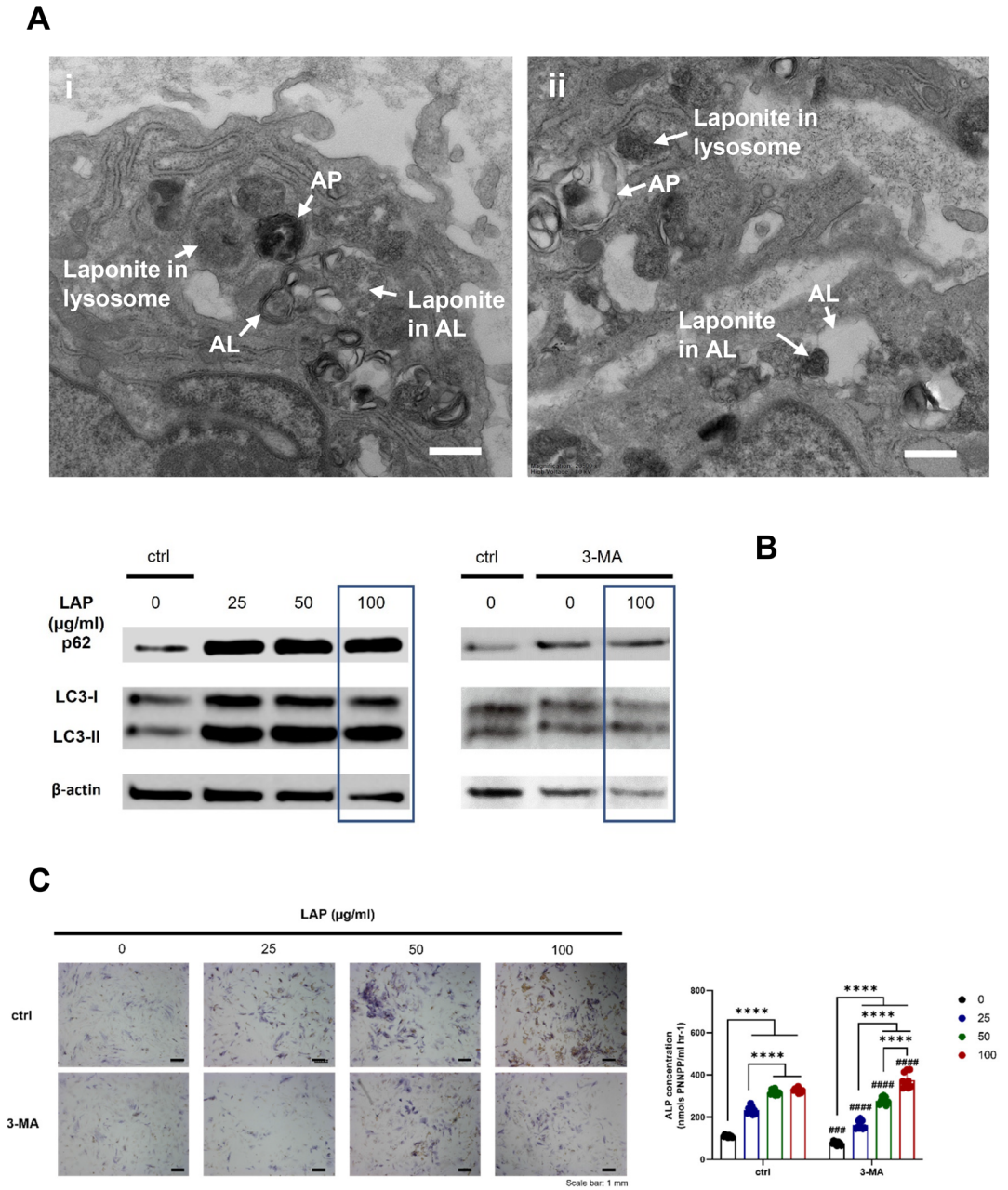

Fig. 8 Effect of internalized nanoclay particles on hBMSCs autophagy. (A) TEM images show nanoclay particles stimulate cell autophagy and colocalize with lamellar/residual bodies in autophagosomes for degradation. Cells were treated with 100 μg mL^{-1} nanoclay dispersion for 3 (i) or 7 days (ii). AP = autophagosome; AL = autolysosome. Images were taken at magnifications of 20 500× using FEI Tecnai T12 Transmission Electron Microscope. Scale bar = 500 nm. (B) Western blot analysis confirm the stimulatory role of nanoclay on hBMSCs autophagy as shown by nanoclay-induced upregulation of autophagy protein markers p62 and LC3 which was attenuated with the addition of 3-MA. (C) Autophagy inhibitor 3-MA was co-administered with nanoclay to test whether autophagy play a role in nanoclay bioactivity assayed *via* ALP activity. No direct association detected between autophagy and nanoclay-promoted ALP activity. Scale bar = 1 mm. *, **, *** and **** indicate *P* values of 0.01, 0.001, and 0.0001, respectively #, ##, ### and #### indicate *P* values of 0.01, 0.001, and 0.0001, respectively, compared to control group with same clay concentration.

nucleus, free in the cytoplasm, or embedded in other cytoplasmic organelles (endoplasmic reticulum, Golgi apparatus & mitochondria), which suggests against the possibility of endosomal/lysosomal escape (at least as intact undegraded particles).[10] However, we observed direct fusion of nanoclay-entrapping lysosomal bodies with plasma membrane indicating some degree of nanoclay exocytosis occurs.

The absence of particles in the cytoplasm, together with the active lysosomal processes observed is consistent with either, or both, of the following scenarios:[10] (i) clay particles

undergo degradation in lysosomes, which is the terminal degradative compartment of the endocytic pathway, causing the release into the cytoplasm of clay dissolution products Mg, Si, Na & Li; (ii) clay particles are exocytosed, through the above discussed routes, either as intact or degraded particles. In fact, we observed various signs of nanoclay particle degradation in lysosomes. For example, TEM imaging showed significant reduction in nanoclay particle size in lysosomes (<10 nm) compared to particles in the extracellular environment or in early endosomes (~30–50 nm). It's worth noting that standard nanoclay particle size in aqueous solution is 25–30 nm and in culture media around 100 nm according to literature.[21,28] Similar results were observed with mesoporous silica in lysosomes and cytoplasm of HUVECs in which particles underwent significant time-dependent reduction in their size (<200 nm) compared to original particles (300–430 nm) initially applied to the cells.[38] The authors inferred particle degradation both in cytoplasm and lysosomes which was confirmed by confocal microscopy and inductively coupled plasma atomic emission spectroscopy (ICP-OES) analysis of cell lysate supernatant.[38] In addition to particle size change, the increase in Si/Mg weight or atomic ratio of lysosomal nanoclay (3.8) compared to early endosomal or extracellular nanoclay (2) is also suggestive of nanoclay degradation. At pH below 9, as for example the lysosomal pH 4.5, H^+ first attack the edge of the nanoclay crystal (Mg–OH)[39] and the octahedral layer undergoes predominant and faster dissolution over the tetrahedral network.[40] This will thus lead to quicker Mg^{2+} release than Si^{4+} and in turn higher Si/Mg peak ratio detected by EDX.

In agreement with the results presented in this study, the degradation of nanoclay nanoparticles at pH < 9 is well documented in literature.[5,28,41] For example, recent work by Tang[42] and Yao[43] *et al.* provided evidence for nanoclay nanorod and nanoplatelet degradation in cell culture media (pH = 7–7.4) as shown by significant time-dependent increase in the concentration of Si, Mg and Li ions in cell culture media extracts obtained from immersing nanoclay-containing nanocomposites for 7 days. Moreover, Brokesh *et al.* reported the vulnerability of nanoclay particles for degradation at both pH 7.4 (mimicking extracellular environment) and pH 5.5 (mimicking endosome microenvironment) in a time-dependent manner.[44] Moreover, anticancer drugs loaded on/in nanoclay followed higher release rate in acidic lysosomal-mimicking pH conditions than in physiological conditions[32,45] which might again be attributed to acid-enhanced nanoparticle degradation under these low pH conditions. The equation for this pH dependent dissolution is shown by Thompson and Butterworth equation below.[28,41,46]

$$\mathrm{Na_{0.8}Si_8Mg_{5.4}Li_{0.4}O_{20}(OH)_4 + 12H^+ + 8H_2O \rightarrow 0.8Na^+ + 8Si(OH)_4 + 5.4Mg^{2+} + 0.4Li^+.}$$

When reviewing the literature we observed that other stem cell populations exhibited a similar interaction pattern with nanoclay although the intracellular journey was not clearly detailed as in our study. For example, Carrow *et al.* and Mihaila *et al.*, reported nanoclay uptake by mesenchymal stem cells and adipose-derived stem cells *via* clathrin-mediated endocytosis and nanoclay colocalization with lysosomes as demonstrated by confocal microscopy.[16,18] Other nanoclay types such as kaolinite and anionic clays, commonly used in drug delivery, are entrapped in lysosome of cancer cells for nanoclay degradation. Together, these data suggest a similar intracellular pathway of nanoclay in other cell types such as cancer and normal cells and necessitate the need to elucidate this pathway in other cell types.[36]

An interesting finding of this study is the indication that cellular uptake of nanoclay induces cell autophagy. This is suggested by the appearance of double membrane vesicles – a typical feature of autophagosomes/autolysosomes[22] and the upregulation of autophagy protein markers in nanoclay-treated cells. Furthermore, nanoclay particles were observed in autolysosomes resulting from fusion of autophagosomes with nanoclay-entrapping lysosomes. Such nanoparticle-induced autophagy was also observed with other nanoparticles such as gold,[11] silica[12] and silver.[35] Interestingly, autophagy, which is a lysosome-based degradative pathway, has been linked to osteoblast differentiation *in vitro* and bone formation *in vivo*[47,48] and various nanoparticles have been shown to stimulated cell osteogenic differentiation through autophagy-induction pathways. For example, addition of autophagy inhibitors 3-methyladenine (MA) and chloroquine (CQ) significantly reversed the gold[11] and silver[49] nanoparticles-enhanced ALP activity and mineralization of mesenchymal stem cells bringing back to control levels compared to nanoparticles alone and silica nanoparticles were found in autolysosomes of differentiating osteoblasts.[12] Interestingly, while nanoclay addition causes a strong upregulation of both ALP activity and autophagy markers, in our hands 3-MA inhibition of autophagy did not appear to influence and ALP response suggesting alternative pathways are at play.[11]

4. Conclusion

This study answers key questions regarding the fate of nanoclay following interaction with human bone marrow stromal cells which is critical for the successful control and manipulation of these nanomaterials not only for the regenerative medicine field but also for biomedical applications in general. Nanoclay was readily internalized by hBMSCs in a time-dependent manner and the amount of nanoclay distributed across the cell culture system was in the order extracellular > intracellular > surface bound. Nanoclay started its intracellular journey through endocytosis followed by entrapment exclusively in endosomal and lysosomal vesicles. This study also provides new evidence that nanoclay undergoes degradation in lysosomes and exocytosis through direct lysosomal fusion with cell membrane and that endocytosis but not autophagy is necessary for the widely reported osteogenic effects of nanoclay on osteoprogenitor cell populations.

5. Materials and methods

5.1. Isolation and culture of human bone marrow stromal cells

Experiments in this study were conducted using human bone marrow stromal cells (hBMSCs). HBMSCs were isolated from femoral bone marrow samples obtained from haematologically normal osteoporotic or osteoarthritic patients undergoing hip replacement surgery at Southampton General Hospital or Spire Hospital Southampton, with the approval of the appropriate Local Research Ethics Committee (LREC 194/99/1). Briefly, bone marrow aspirate from patient's femur undergone repeated washes/perfusion steps with α-MEM followed by centrifugation at 1100 rpm for 5 minutes. The cell pellet was resuspended in α-MEM and filtered through 70 μm cell strainer to isolate the cell population from the residual bone chips and remaining unwanted tissues. Cells were seeded at low density (5×10^3 cells per cm^2) in growth medium (α-MEM with supplements of 10% (v/v) FBS and 100 μg ml^{-1} penicillin/streptomycin) and incubated in monolayer at 37 °C and under humidified 5% CO_2 for 3 hours. Culture media change was performed to remove nonadherent cell fraction (red blood cells) while the adherent cells were further grown under the same conditions for 12–14 days, before being passaged for culture expansion. Cells with colony-forming ability were harvested and used in subsequent experiments. Culture medium was changed every 3–4 days. For all experiments, the obtained hBMSCs were used before passage 4.

5.2. Preparation of nanoclay dispersion in cell culture medium

Nanoclay used in this study (XLG; batch number SR4871) was kindly gifted from BYK-ALTANA. Freshly prepared nanoclay dispersions were used for all experiments. Briefly, nanoclay powder (standard/unlabeled or labelled with Rhodamine B isothiocyanate) was dispersed in d-H_2O (18.2 MΩ) at concentration of 5% (w/v) and filter sterilised before being applied to cell culture medium. Cell culture media (basal or osteogenic) was allowed to stir at 700 rpm forming a vortex then nanoclay/H_2O solution was added in a very slow manner, to avoid particle agglomeration, up to a final conc. of 100 μg mL^{-1}. For negative control, nanoclay-free H_2O was added. The resultant nanoclay dispersions in cell culture media were allowed to stir for 30 minutes before being diluted to the appropriate concentration in media and applied to cells. Basal media consisted of α-MEM (Lonza) containing 10% FBS and 100 μg ml^{-1} penicillin/streptomycin (Sigma), while osteogenic media was prepared of basal media supplemented with 100 μM ascorbate-2-phosphate, 10 mM β-glycerophosphate and 10 nM dexamethasone (Sigma).

5.3. Effect of nanoclay on cell viability

Nanoclay cytotoxicity was determined using WST-1 colorimetric assay (Roche, Germany). The technique is based on the cleavage of tetrazolium salts to formazan dye by mitochondrial dehydrogenases produced by viable cells. Cells were seeded in clear flat-bottom 96-well plates at varying densities of 3×10^3–12×10^3 cells per cm^2 in basal medium and allowed to adhere for 24 hours at 37 °C and 5% CO_2. Next, existing culture media was changed with fresh basal media supplemented with nanoclay particles at a final conc. of 0–1000 μg mL^{-1}. After 24 hours incubation, 10 μL WST1 reagent was added for each well and incubated for 1 hour. The absorbance was measured using EL-800 Universal Microplate Reader (BioTek Instruments Inc., Winooski, USA) at 450 nm. The absorbance/colour intensity produced by formazan product correlates with the number of viable cells in the samples.

The biocompatibility of nanoclay particles was confirmed using confocal and phase contrast microscopy. Cells were seeded at 10^4 cells per cm^2 and allowed to adhere overnight then treated with 100 μg mL^{-1} and cells were imaged following 24 h of nanoclay exposure.

5.4. Tracking nanoclay uptake kinetics using confocal microscopy

For assessing nanoclay uptake kinetics by hBMSCs, cells were treated with Rhodamine B-labelled nanoclay particles and imaged using confocal microscopy. First, nanoclay powder was fluorescently labelled with Rhodamine B isothiocyanate RBITC dye (20653, Cayman Chemicals, USA). Briefly, 0.5 g nanoclay powder was dispersed in 25 mL of 1 mg mL^{-1} RBITC solution, prepared in anhydrous DMSO (ThermoFisher). The mixture was kept under continuous stirring overnight in dark conditions. Repeated washing-centrifugation steps with absolute ethanol were performed until supernatant appeared colorless indicating complete removal of excess dye. The resulting nanoclay-RBITC powder was separated *via* filtration using Buckner funnel, air dried at room temperature and stored, protected from light, until further use.

HBMSCs were seeded at density 10^4 cells per cm^2 in a 24-well plate on # 1.5 sterilized glass coverslips. Cells allowed to adhere in basal medium for 24 hours. RBITC-labelled nanoclay dispersion in basal culture medium at 100 μg mL^{-1} was prepared as previously mentioned in section 5.2. Cell culture media was replaced with nanoclay-containing *vs.* nanoclay-free basal media for clay-treated *vs.* negative control groups, respectively. Cells were incubated with nanoclay at 37 °C, 5% CO_2 for 1, 3 and 7 days. For cells exposed to nanoclay for 7 days, nanoclay was added at a single dose (time point 0) and cells incubated with nanoclay for complete 7 days without media change to allow enough time for the particles to be processed by the cells.

At each selected timepoint, culture media was discarded and cells were washed twice with phosphate buffered saline (DPBS). Then, cells were incubated with Cell Mask™ Deep Red plasma membrane stain (C10046, Invitrogen), at 1/1000 dilution in DPBS of 5 mg mL^{-1} stock solution in DMSO, for 10 minutes at 37 °C. Cell mask stain was removed, cells were washed twice with DPBS and detached though incubation with trypsin/EDTA 1× for 5 minutes at 37 °C, 5% CO_2. Basal media

was added to detached cells to deactivate trypsin action then transferred to Eppendorf tube for centrifugation at 400 RCF for 5 minutes at 21 °C. Supernatant was discarded and cell pellet was resuspended and fixed in 4% paraformaldehyde and for 10 minutes at room temperature. Fixed cell suspension was transferred into μ-Slide 8 Well Glass Bottom chamber (80827, Ibidi). Cells were imaged by Leica TCS-SP8 Confocal Microscope equipped with Leica LAS-X software at the following excitation/emission wavelengths: 570/595 nm for RBITC and 649/666 nm for cell mask deep red stain.

5.5. Tracking mechanism of nanoclay uptake by hBMSCs and role of endocytosis in nanoclay bioactivity

For assessing the effect of CPZ on nanoclay endocytosis, hBMSCs were treated with and without 5 μg mL^{-1} for 2 hours. Then, nanoclay particles were dispersed in basal culture media at final conc. of 100 μg mL^{-1} and supplemented with either CPZ or dH_2O for CPZ-treated and CPZ-free sample groups respectively. Therefore, 3 sample groups were generated including cells alone (without nanoclay & without CPZ), cells + nanoclay (without CPZ) and cells + nanoclay + CPZ. Cells were cultured for 24 hours at 37 °C, 5% CO_2 followed by confocal imaging of cell nucleus (DAPI), nanoclay (Rhodamine B), and cell membrane (cell mask deep red) as described above. DAPI was excited at 358 nm.

For investigating the effect of endocytosis inhibition on nanoclay induction of alkaline phosphatase ALP activity, hBMSCs were seeded at 10^4 cells per cm^2 in basal medium and allowed to adhere overnight. Culture media was discarded, cells were washed twice with DPBS then incubated with or without CPZ in basal media at 5 μg mL^{-1} for 2 h. Then, nanoclay nanoparticles were dispersed in basal and osteogenic culture media at final conc. of 100 μg mL^{-1} which then was supplemented with either CPZ (final conc. is 5 μg mL^{-1}) or dH_2O for CPZ-treated and CPZ-free sample groups respectively. Therefore, 4 sample groups were generated including cells alone (without nanoclay & without CPZ), cells + CPZ (without nanoclay), cells + nanoclay (without CPZ) and cells + nanoclay + CPZ. Then, the as-prepared basal and osteogenic culture media with or without nanoclay/CPZ were added to the corresponding cell wells and incubated at 37 °C, 5% CO_2 for three days. At day 3, ALP activity was quantified using an end-point colorimetric assay based on the conversion of *p*-nitrophenol phosphate (*p*NPP) to yellow *p*-nitrophenol (*p*NP) by ALP enzyme according to manufacturer protocol.

5.6. Quantifying intracellular *vs.* extracellular nanoclay using ICPMS

HBMSCs were seeded in 6-well plates at density of 10^4 cells per cm^2 in basal medium and left to adhere for 24 hours at 37 °C and 5% CO_2. Next, existing culture media was changed with fresh basal media supplemented with nanoclay nanoparticles at a final concentration of 100 μg mL^{-1}. For negative control nanoclay-free medium was used. Cells were incubated with nanoclay at 37 °C, 5% CO_2 for 7 days. Selected time points are day 1, 3 and 7 and each sample was run in triplicates.

At each selected time point, cell culture media was collected in Falcon tubes – this represents extracellular nanoclay free in the system. Then, cells were washed 3 times with DPBS to collect non-internalised particles adhered on cell membrane. To collect internalized nanoclay particles cell monolayer was detached by incubation with trypsin/EDTA 1× for 5 minutes. Cell suspension was transferred to collection tubes, mixed very well and cells were counted using the haemocytometer chamber. Centrifugation was performed at 400 RCF for 5 min at 21 °C to separate the cells. Supernatant was removed and cell pellet was resuspended in dH_2O. It's worth noting that the above-mentioned steps were performed in clean fume hood to avoid contamination by atmospheric particulates which might contain one or more the elements under investigation such as silicon.

For sample digestion and analysis by ICPMS, each sample was homogenised by vortexing and transferred to digestion Teflon vessel. Then, each sample was soaked in conc. HNO_3 and 30% H_2O_2 overnight and heated gradually to 130 °C until the solution was colourless and clear indicating complete sample digestion. Vessels containing HNO_3 and H_2O_2 but no nanoclay was used as blank controls. Samples cooled down and diluted with In/Re spiked 3% HNO_3 (dilution factor = 10). Finally, the Si and Li content were analysed using Thermo Scientific ELEMENT XR HR-ICPMS with indium as an internal standard. The amount/percentage of nanoclay (LAP) internalized, adhered on cell membrane, and remained free in extracellular space was calculated according to the following formula:

$$\text{Conc. of LAP (pg per cell)} = \text{measured conc. of Li(pg per cell)} \times (1/0.0027).$$

Based on LAP structural formula $Na^{+}_{0.7}$ $[(Mg_{5.5}Li_{0.3})Si_8O_{20}(OH)_4]^{-0.7}$ each 1 pg LAP contain 0.0027 pg Li.

For converting the measured nanoclay conc. per cell into number of nanoclay particles per cell, we followed the calculations below:

The unit cell formula for nanoclay is: $Na^{+}_{0.7}$ $[(Mg_{5.5}Li_{0.3})Si_8O_{20}(OH)_4]^{-0.7}$

The M.W of each unit-cell = 764.55379 g mol^{-1} (calculated from the above unit-cell formula)

Therefore, each 764.55379 g nanoclay contains 6.022×10^{23} unit cells (Avogadro's number)

Therefore, for the used concentration (100 μg ml^{-1}), each 1 ml contains $(0.0001\ g \times 6.022 \times 10^{23})/(764.55379\ g) = 7.876 \times 10^{16}$ unit cells

Considering that, and according to literature[39,50] every nanoclay particle contains around 1000 unit cells, then there will be 7.876×10^{13} nanoclay particles per ml for the previous clay conc. (100 μg ml^{-1}). And the nanoclay particle density = $(7.876 \times 10^{13})/(0.0001\ g) = 7.876 \times 10^{17}$ nanoclay particle per gram of nanoclay, which is in good agreement with Felbeck *et al.*[51] (7.04×10^{17} particle per g), considering nanoclay density of 2.58 g cm^{-3} and unit cell dimensions of $a = 0.53 \times b = 0.92 \times c = 1$ nm, $\beta = 99°$.

No. of nanoclay particles per cell (particle per cell) = measured conc. of nanoclay (ng per cell) × 7.876 × 10^{17}.

It's worth noting that a parallel study was performed to determine which element (Si *vs.* Li) best fit as a reliable marker for nanoclay concentration measurement by ICPMS. Nanoclay standards (0–100 μg mL^{-1}) were prepared in basal culture media as discussed in section 4.2 and the concentration of Si and Li analysed by ICPMS as described above. Lithium was selected as it showed a higher degree of correlation (R^2 = 0.98) and discrete difference between expected and measured value (data shown in ESI†).

5.7. Tracking intracellular journey and fate of nanoclay using TEM-EDX

Cellular uptake, intracellular trafficking and fate of nanoclay particles were investigated using FEI Tecnai12 (ThermoFisher, Netherlands) coupled with energy dispersive X-ray unit based on protocol developed by the biomedical imaging unit, University of Southampton and modified from an earlier study.[52] HBMSCs were seeded in 6-well plates at density of 5 × 10^5 cells per well in basal media and incubated for 24 hours. Next day, culture media was replaced with nanoclay-containing (100 μg mL^{-1}) and nanoclay-free fresh basal media for the clay-treated and negative control samples, respectively. Samples were run in triplicate and incubated with nanoclay at 37 °C and 5% CO_2 for 1, 3 and 7 days. Samples were processed at day 1, 3 and 7 for TEM-EDX imaging and analysis as discussed below.

At each selected time point, cell culture media was discarded, cells were washed with phosphate buffered saline and incubated with trypsin/EDTA 1× for 5 min at 37 °C, 5% CO_2 to detach cell monolayer. Basal media was added to deactivate trypsin action and cell suspension was transferred to 2 mL collection tubes for centrifugation at 400 RCF for 5 min at 21 °C to collect cell pellet. Supernatant was discarded and cell pellet fixed in 3% glutaraldehyde and 4% formaldehyde in 0.1 M PIPES buffer at pH 7.2 for 1 hour at room temperature. Samples moved to sectioning and imaging in the biomedical imaging unit, University of Southampton.

For sample processing/sectioning, cells were rinsed twice (10 min per time) in 0.1 M PIPES buffer at pH 7.2 followed by post-fixation in 1% osmium tetroxide in 0.1 M PIPES buffer at pH 7.2 for 1 hour. Samples were rinsed twice again in 0.1 M PIPES buffer at pH 7.2 (10 min per time) followed by distilled water and 2% aqueous uranyl acetate for 30 seconds and 20 minutes, respectively. Next, the samples undergone dehydration in graded series of ethanol and eventually embedded in epoxy resin before being sectioned/cut into 90 nm sections using ultra-microtome. Ultrathin sections were examined using TEM-EDX at an accelerating voltage of 60 kV and magnifications 6–60 000×.

5.8. Western blot analysis of cell autophagy response to nanoclay

HBMSCs were seeded at density of 5 × 10^6 cells per cm^2 per Petri dish in basal medium and left to adhere for 24 hours at 37 °C and 5% CO_2. Next day, basal culture media was replaced with fresh nanoclay containing *vs.* nanoclay-free media used as control. Nanoclay doses tested were 25, 50 and 100 μL. Cells were allowed to interact with nanoclay for 3 days then cell lysate was collected for analyzing expression of p62, LC3-I and LC3-II. B-Actin was used as internal control. To test for a potential link between autophagy activation and nanoclay osteogenic bioactivity, we applied 3-MA autophagy inhibitor at 0.5 mM. Cells were treated with nanoclay in absence and presence of 0.5 mM and ALP activity was assayed at day 3 using an end-point colorimetric assay as described above.

5.9. Statistical analysis

Statistical analysis was performed using GraphPad Prism 8.4.3. Data in graphs are expressed as the mean ± SD. ICPMS experiments were performed in triplicate using cells from a single donor source. Comparisons between experiment groups were performed using one-way ANOVA. Tukey's multiple comparisons test was used to determine significant differences between groups, where significance is set at $P < 0.05$.

Conflicts of interest

Prof. Jonathan I. Dawson and Prof. Richard O. C. Oreffo are founders and shareholders in Renovos Biologics Ltd. which is a spin-out company from the University of Southampton seeking to commercialise the application of clay nanoparticles in regenerative medicine. The remaining authors declare no competing interests.

Acknowledgements

This study is supported by Dr Jonathan I. Dawson EPSRC fellowship (grant number EP/L010259/1). Dr Mohamed Mousa would like to acknowledge the Faculty of Engineering and the Environment, University of Southampton and BYK-ALTANA for funding his PhD. The results presented in this study are part of Dr Mohamed Mousa's PhD thesis which could be accessed through the University of Southampton Institutional Repository: https://eprints.soton.ac.uk/448875/1/PhD_Thesis_MM_28871499.pdf.

References

1 K. Li, S. Wang, S. Wen, Y. Tang, J. Li, X. Shi and Q. Zhao, Enhanced in vivo antitumor efficacy of doxorubicin encapsulated within nanoclay nanodisks, *ACS Appl. Mater. Interfaces*, 2014, **6**(15), 12328–12334, DOI: 10.1021/am502094a.

2 M. Jafarbeglou, M. Abdouss, A. M. Shoushtari and M. Jafarbeglou, Clay nanocomposites as engineered drug delivery systems, *RSC Adv.*, 2016, **6**(55), 50002–50016, DOI: 10.1039/c6ra03942a.

3 J. I. Dawson and R. O. C. Oreffo, Clay: New opportunities for tissue regeneration and biomaterial design, *Adv. Mater.*, 2013, **25**(30), 4069–4086, DOI: 10.1002/adma.201301034.

4 M. Mousa, N. D. Evans, R. O. C. Oreffo and J. I. Dawson, Clay nanoparticles for regenerative medicine and biomaterial design: A review of clay bioactivity, *Biomaterials*, 2018, **159**, 204–214, DOI: 10.1016/j.biomaterials.2017.12.024.

5 A. K. Gaharwar, L. M. Cross, C. W. Peak, K. Gold, J. K. Carrow, A. Brokesh and K. A. Singh, 2D Nanoclay for Biomedical Applications: Regenerative Medicine, Therapeutic Delivery, and Additive Manufacturing, *Adv. Mater.*, 2019, **31**(23), 1900332–1900332, DOI: 10.1002/adma.201900332.

6 A. K. Gaharwar, S. M. Mihaila, A. Swami, A. Patel, S. Sant, R. L. Reis, A. P. Marques, M. E. Gomes and A. Khademhosseini, Bioactive silicate nanoplatelets for osteogenic differentiation of human mesenchymal stem cells, *Adv. Mater.*, 2013, **25**(24), 3329–3336, DOI: 10.1002/adma.201300584.

7 P. Shi, Y. H. Kim, M. Mousa, R. R. Sanchez, R. O. C. Oreffo and J. I. Dawson, Self-Assembling Nanoclay Diffusion Gels for Bioactive Osteogenic Microenvironments, *Adv. Healthcare Mater.*, 2018, **7**(15), 1800331–1800331, DOI: 10.1002/adhm.201800331.

8 S. Behzadi, V. Serpooshan, W. Tao, M. A. Hamaly, M. Y. Alkawareek, E. C. Dreaden, D. Brown, A. M. Alkilany, O. C. Farokhzad and M. Mahmoudi, Cellular uptake of nanoparticles: Journey inside the cell, *Chem. Soc. Rev.*, 2017, **46**(14), 4218–4244, DOI: 10.1039/c6cs00636a.

9 T. G. Iversen, T. Skotland and K. Sandvig, Endocytosis and intracellular transport of nanoparticles: Present knowledge and need for future studies, *Nano Today*, 2011, **6**(2), 176–185, DOI: 10.1016/j.nantod.2011.02.003.

10 N. D. Donahue, H. Acar and S. Wilhelm, Concepts of nanoparticle cellular uptake, intracellular trafficking, and kinetics in nanomedicine, *Adv. Drug Delivery Rev.*, 2019, **143**, 68–96, DOI: 10.1016/j.addr.2019.04.008.

11 Y. Zhang, N. Kong, Y. Zhang, W. Yang and F. Yan, Size-dependent effects of gold nanoparticles on osteogenic differentiation of human periodontal ligament progenitor cells, *Theranostics*, 2017, **7**(5), 1214–1224, DOI: 10.7150/thno.17252.

12 S. W. Ha, M. Neale Weitzmann and G. R. Beck, Bioactive silica nanoparticles promote osteoblast differentiation through stimulation of autophagy and direct association with LC3 and p62, *ACS Nano*, 2014, **8**(6), 5898–5910, DOI: 10.1021/nn5009879.

13 T. Pan, W. Song, H. Gao, T. Li, X. Cao, S. Zhong and Y. Wang, MiR-29b-Loaded Gold Nanoparticles Targeting to the Endoplasmic Reticulum for Synergistic Promotion of Osteogenic Differentiation, *ACS Appl. Mater. Interfaces*, 2016, **8**(30), 19217–19227, DOI: 10.1021/acsami.6b02969.

14 A. Panariti, G. Miserocchi and I. Rivolta, The effect of nanoparticle uptake on cellular behavior: Disrupting or enabling functions?, *Nanotechnol., Sci. Appl.*, 2012, **5**(1), 87–100, DOI: 10.2147/NSA.S25515.

15 A. Albanese, P. S. Tang and W. C. W. Chan, The effect of nanoparticle size, shape, and surface chemistry on biological systems, *Annu. Rev. Biomed. Eng.*, 2012, **14**, 1–16, DOI: 10.1146/annurev-bioeng-071811-150124.

16 S. M. Mihaila, A. K. Gaharwar, R. L. Reis, A. Khademhosseini, A. P. Marques and M. E. Gomes, The osteogenic differentiation of SSEA-4 sub-population of human adipose derived stem cells using silicate nanoplatelets, *Biomaterials*, 2014, **35**(33), 9087–9099, DOI: 10.1016/j.biomaterials.2014.07.052.

17 T. Li, Z. L. Liu, M. Xiao, Z. Z. Yang, M. Z. Peng, C. D. Li, X. J. Zhou and J. W. Wang, Impact of bone marrow mesenchymal stem cell immunomodulation on the osteogenic effects of nanoclay, *Stem Cell Res. Ther.*, 2018, **9**(1), 100–100, DOI: 10.1186/s13287-018-0818-0.

18 J. K. Carrow, L. M. Cross, R. W. Reese, M. K. Jaiswal, C. A. Gregory, R. Kaunas, I. Singh and A. K. Gaharwar, Widespread changes in transcriptome profile of human mesenchymal stem cells induced by two-dimensional nanosilicates, *Proc. Natl. Acad. Sci. U. S. A.*, 2018, **115**(17), E3905–E3913, DOI: 10.1073/pnas.1716164115.

19 C. Gottstein, G. Wu, B. J. Wong and J. A. Zasadzinski, Precise quantification of nanoparticle internalization, *ACS Nano*, 2013, **7**(6), 4933–4945, DOI: 10.1021/nn400243d.

20 M. Mousa, J. A. Milan, O. Kelly, J. Doyle, N. D. Evans, R. O. C. Oreffo and J. I. Dawson, The role of lithium in the osteogenic bioactivity of clay nanoparticles, *Biomater. Sci.*, 2021, 3150–3161, DOI: 10.1039/d0bm01444c.

21 L. M. Cross, J. K. Carrow, X. Ding, K. A. Singh and A. K. Gaharwar, Sustained and Prolonged Delivery of Protein Therapeutics from Two-Dimensional Nanosilicates, *ACS Appl. Mater. Interfaces*, 2019, **11**(7), 6741–6750, DOI: 10.1021/acsami.8b17733.

22 E. L. Eskelinen, To be or not to be? Examples of incorrect identification of autophagic compartments in conventional transmission electron microscopy of mammalian cells, *Autophagy*, 2008, **4**(2), 257–260, DOI: 10.4161/auto.5179.

23 K. Das, K. Rawat and H. B. Bohidar, Surface patch binding induced interaction of anisotropic nanoclays with globular plasma proteins, *RSC Adv.*, 2016, **6**(106), 104117–104125, DOI: 10.1039/C6RA11669H.

24 S. T. Stealey, A. K. Gaharwar, N. Pozzi and S. P. Zustiak, Development of Nanosilicate-Hydrogel Composites for Sustained Delivery of Charged Biopharmaceutics, *ACS Appl. Mater. Interfaces*, 2021, **13**(24), 27880–27894, DOI: 10.1021/acsami.1c05576, from NLM.

25 M. Zhu, G. Nie, H. Meng, T. Xia, A. Nel and Y. Zhao, Physicochemical properties determine nanomaterial cellular uptake, transport, and fate, *Acc. Chem. Res.*, 2013, **46**(3), 622–631, DOI: 10.1021/ar300031y.

26 R. R. Arvizo, O. R. Miranda, M. A. Thompson, C. M. Pabelick, R. Bhattacharya, J. David Robertson, V. M. Rotello, Y. S. Prakash and P. Mukherjee, Effect of nanoparticle surface charge at the plasma membrane and beyond, *Nano Lett.*, 2010, **10**(7), 2543–2548, DOI: 10.1021/nl101140t.

27 S. Zhang, J. Li, G. Lykotrafitis, G. Bao and S. Suresh, Size-dependent endocytosis of nanoparticles, *Adv. Mater.*, 2009, **21**(4), 419–424, DOI: 10.1002/adma.200801393.

28 D. W. Thompson and J. T. Butterworth, The nature of LAPONITE® and its aqueous dispersions, *J. Colloid Interface Sci.*, 1992, **151**(1), 236–243, DOI: 10.1016/0021-9797(92)90254-J.
29 A. Chaudhuri, G. Battaglia and R. Golestanian, The effect of interactions on the cellular uptake of nanoparticles, *Phys. Biol.*, 2011, **8**(4), 046002–046002, DOI: 10.1088/1478-3975/8/4/046002.
30 B. Halamoda-Kenzaoui, M. Ceridono, P. Urbán, A. Bogni, J. Ponti, S. Gioria and A. Kinsner-Ovaskainen, The agglomeration state of nanoparticles can influence the mechanism of their cellular internalisation, *J. Nanobiotechnol.*, 2017, **15**(1), 1–15, DOI: 10.1186/s12951-017-0281-6.
31 H. Jin, D. A. Heller, R. Sharma and M. S. Strano, Size-dependent cellular uptake and expulsion of single-walled carbon nanotubes: Single particle tracking and a generic uptake model for nanoparticles, *ACS Nano*, 2009, **3**(1), 149–158, DOI: 10.1021/nn800532m.
32 S. Wang, Y. Wu, R. Guo, Y. Huang, S. Wen, M. Shen, J. Wang and X. Shi, nanoclay nanodisks as an efficient platform for doxorubicin delivery to cancer cells, *Langmuir*, 2013, **29**(16), 5030–5036, DOI: 10.1021/la4001363.
33 B. D. Chithrani, A. A. Ghazani and W. C. W. Chan, Determining the size and shape dependence of gold nanoparticle uptake into mammalian cells, *Nano Lett.*, 2006, **6**(4), 662–668, DOI: 10.1021/nl052396o.
34 C. Yi, D. Liu, C. C. Fong, J. Zhang and M. Yang, Gold nanoparticles promote osteogenic differentiation of mesenchymal stem cells through p38 MAPK pathway, *ACS Nano*, 2010, **4**(11), 6439–6448, DOI: 10.1021/nn101373r.
35 C. Greulich, J. Diendorf, T. Simon, G. Eggeler, M. Epple and M. Köller, Uptake and intracellular distribution of silver nanoparticles in human mesenchymal stem cells, *Acta Biomater.*, 2011, **7**(1), 347–354, DOI: 10.1016/j.actbio.2010.08.003.
36 H. E. Chung, D. H. Park, J. H. Choy and S. J. Choi, Intracellular trafficking pathway of layered double hydroxide nanoparticles in human cells: Size-dependent cellular delivery, *Appl. Clay Sci.*, 2012, **65–66**, 24–30, DOI: 10.1016/j.clay.2012.06.007.
37 J. P. Luzio, P. R. Pryor and N. A. Bright, *Lysosomes: Fusion and function*, 2007, vol. 8, pp. 622–632.
38 W. Zhai, C. He, L. Wu, Y. Zhou, H. Chen, J. Chang and H. Zhang, Degradation of hollow mesoporous silica nanoparticles in human umbilical vein endothelial cells, *J. Biomed. Mater. Res., Part B*, 2012, **100**(5), 1397–1403, DOI: 10.1002/jbm.b.32711.
39 R. P. Mohanty and Y. M. Joshi, Chemical stability phase diagram of aqueous LAPONITE® dispersions, *Appl. Clay Sci.*, 2016, **119**, 243–248, DOI: 10.1016/j.clay.2015.10.021.
40 T. A. Sokolova, Decomposition of clay minerals in model experiments and in soils: Possible mechanisms, rates, and diagnostics (analysis of literature), *Eurasian Soil Sci.*, 2013, **46**(2), 182–197, DOI: 10.1134/S1064229313020130.
41 S. Jatav and Y. M. Joshi, Chemical stability of nanoclay in aqueous media, *Appl. Clay Sci.*, 2014, **97–98**, 72–77, DOI: 10.1016/j.clay.2014.06.004.
42 L. Tang, W. Wei, X. Wang, J. Qian, J. Li, A. He, L. Yang, X. Jiang, X. Li and J. Wei, nanoclay nanorods regulating degradability, acidic-alkaline microenvironment, apatite mineralization and MC3T3-E1 cells responses to poly(butylene succinate) based bio-nanocomposite scaffolds, *RSC Adv.*, 2018, **8**(20), 10794–10805, DOI: 10.1039/c7ra13452e.
43 Q. Yao, K. E. Fuglsby, X. Zheng and H. Sun, Nanoclay-functionalized 3D nanofibrous scaffolds promote bone regeneration, *J. Mater. Chem. B*, 2020, **8**(17), 3842–3851, DOI: 10.1039/c9tb02814e.
44 A. M. Brokesh, L. M. Cross, A. L. Kersey, A. Murali, C. Richter, C. A. Gregory, I. Singh and A. K. Gaharwar, Dissociation of nanosilicates induces downstream endochondral differentiation gene expression program, *Sci. Adv.*, 2022, **8**(17), eabl9404, DOI: 10.1126/sciadv.abl9404.
45 M. Gonçalves, P. Figueira, D. Maciel, J. Rodrigues, X. Qu, C. Liu, H. Tomás and Y. Li, PH-sensitive nanoclay/doxorubicin/alginate nanohybrids with improved anticancer efficacy, *Acta Biomater.*, 2014, **10**(1), 300–307, DOI: 10.1016/j.actbio.2013.09.013.
46 I. Bibi, B. Singh and E. Silvester, Dissolution kinetics of soil clays in sulfuric acid solutions: Ionic strength and temperature effects, *Appl. Geochem.*, 2014, **51**, 170–183, DOI: 10.1016/j.apgeochem.2014.10.004.
47 F. Liu, F. Fang, H. Yuan, D. Yang, Y. Chen, L. Williams, S. A. Goldstein, P. H. Krebsbach and J. L. Guan, Suppression of autophagy by FIP200 deletion leads to osteopenia in mice through the inhibition of osteoblast terminal differentiation, *J. Bone Miner. Res.*, 2013, **28**(11), 2414–2430, DOI: 10.1002/jbmr.1971.
48 N. Mizushima and B. Levine, Autophagy in mammalian development and differentiation, *Nat. Cell Biol.*, 2010, **12**(9), 823–830, DOI: 10.1038/ncb0910-823.
49 W. He, Y. Zheng, Q. Feng, T. A. Elkhooly, X. Liu, X. Yang, Y. Wang and Y. Xie, Silver nanoparticles stimulate osteogenesis of human mesenchymal stem cells through activation of autophagy, *Nanomedicine*, 2020, **15**(4), 337–353, DOI: 10.2217/nnm-2019-0026.
50 L. Bippus, M. Jaber and B. Lebeau, nanoclay and hybrid surfactant/LAPONITE® particles processed as spheres by spray-drying, *New J. Chem.*, 2009, **33**(5), 1116–1126, DOI: 10.1039/b820429b.
51 T. Felbeck, S. Mundinger, M. M. Lezhnina, M. Staniford, U. Resch-Genger and U. H. Kynast, Multifold fluorescence enhancement in nanoscopic fluorophore-clay hybrids in transparent aqueous media, *Chem. – Eur. J.*, 2015, **21**(20), 7582–7587, DOI: 10.1002/chem.201406416.
52 A. M. Schrand, J. J. Schlager, L. Dai and S. M. Hussain, Preparation of cells for assessing ultrastructural localization of nanoparticles with transmission electron microscopy, *Nat. Protoc.*, 2010, **5**(4), 744–757, DOI: 10.1038/nprot.2010.2.